Journal of Alloys and Compounds 527 (2012) –xxx

Contents lists available at SciVerse ScienceDirect

Journal of Alloys and Compounds

journal homepage: www.elsevier.com/locate/jallcom

Effect of cooling rate on the bending plasticity of $Zr_{55}Al_{10}Ni_5Cu_{30}$ bulk metallic glass

Y. Hu[a,b], H.H. Yan[b], T. Lin[a], J.F. Li[a,*], Y.H. Zhou[a]

[a] State Key Laboratory of Metal Matrix Composites, School of Materials Science and Engineering, Shanghai Jiao Tong University, Shanghai 200240, PR China
[b] School of Materials Science and Engineering, Taiyuan University of Science and Technology, Taiyuan 030024, PR China

ARTICLE INFO

Article history:
Received 31 December 2011
Received in revised form 29 January 2012
Accepted 18 February 2012
Available online xxx

Keywords:
Metallic glass
Microstructure
Plasticity
Cooling rate

ABSTRACT

The effect of cooling rate on the bending plasticity of $Zr_{55}Al_{10}Ni_5Cu_{30}$ bulk metallic glass was investigated by varying the thickness of the as-cast sample. It turned out that as the thickness of the as-cast sample increases from 1 to 3 mm, short-range ordering in the microstructures is enhanced until noticeable nanocrystallization occurs in the thickest sample, but the bending plasticity measured under the same test specification first decreases and then increases. It is suggested that both free volume and structural heterogeneity dominate the plasticity of metallic glasses.

1. Introduction

Bulk metallic glasses (BMGs) possess high strength, hardness and elastic deformation limit due to their random atomic structure and concomitant lack of dislocations and associated slip planes [1–5]. However, during compressive or tensile testing at temperatures far below the glass transition temperature, they often break abruptly along a very narrow shear band, and exhibit little global plasticity [2,4]. Such a catastrophic fracture severely limits their application as structural materials. The plasticity of BMGs can be enhanced by introducing nanoscale compositional heterogeneities via phase separation [6–8] or dispersions of embedded nanocrystals [9–14]. However, recent investigations showed that the plastic strain of some monolithic BMGs could also be remarkably improved by enhancing the homogeneity in microstructure through high cooling rate [15–17], multiple remelting of master ingot [18], appropriate casting temperature [19] or flux treatment of alloy melt [20]. These results seem to suggest that BMGs would experience a nonmonotonic change in plasticity while the microstructure changes from disorder to order. In order to verify such inference, $Zr_{55}Al_{10}Ni_5Cu_{30}$ BMG samples were prepared under different effective cooling rates by varying the as-cast thicknesses, followed by bending test. A "large–small–large" transition in bending plasticity was observed with increasing the thickness. Moreover, it was suggested that a full amorphous structure with high ordering degree is detrimental to bending plasticity.

2. Experimental procedures

The master alloy ingots of $Zr_{55}Al_{10}Ni_5Cu_{30}$ were prepared by arc melting the pure metals in a water-cooled copper crucible under a Ti-gettered argon atmosphere. The ingots were remelted four times to ensure chemical homogeneity, and then suction cast into water-cooled copper molds to form plates of 1 mm × 10 mm × 60 mm, 2 mm × 10 mm × 60 mm, and 3 mm × 10 mm × 60 mm, respectively. Three plates were cast for each size. Bend specimens of 1 mm × 3 mm × 40 mm (thickness × width × length) were cut from the as-cast plates using a diamond saw, followed by machining away the excessive parts symmetrically in the thickness direction and polishing the surfaces. For simplification, hereafter both the as-cast plates of 1, 2 and 3 mm thickness and the bend specimens machined from them are expressed using T-1, T-2 and T-3, respectively.

A Thermo ARL X-ray diffractometer (XRD) with Cu-K_α radiation and a JEOL JEM-2100F high resolution transmission electron microscope (HRTEM) were employed to identify the structure of the as-cast samples. Thermal analyses were performed using a Perkin-Elmer Pyris Diamond differential scanning calorimeter (DSC) at 20 K/min under a flow of high-purity Ar atmosphere. A Zwick/Roell Z10 testing machine was used for the three-point bending test, with a support span of 20 mm and a cross head speed of 0.64 mm/min. After bending, the specimen surfaces were examined with a JEOL JSM-6460 scanning electron microscope (SEM).

3. Experimental results

All the as-cast plates were prepared under the same melting and casting conditions. A smaller thickness of the plate means a higher cooling rate during solidification, which in turn results in differences in the microstructure. Although the XRD patterns of all the as-cast plates consist of the broad diffuse diffraction peaks associated with amorphous structures (the results are not shown

* Corresponding author. Tel.: +86 21 54748530; fax: +86 21 54748530.
E-mail address: jfli@sjtu.edu.cn (J.F. Li).

0925-8388/$ – see front matter © 2012 Elsevier B.V. All rights reserved.
doi:10.1016/j.jallcom.2012.02.126

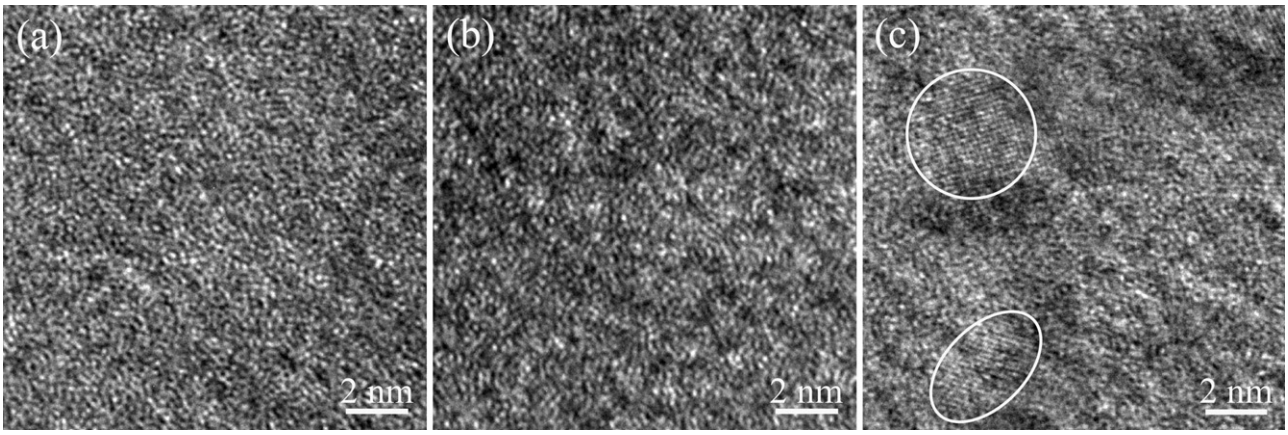

Fig. 1. HRTEM images of the as-cast plates of 1 mm (a), 2 mm (b) and 3 mm (c) thicknesses.

here), HRTEM observations revealed that one plate is different from another in microstructure if their thicknesses are different. A set of HRTEM images are shown in Fig. 1. One sees that both the T-1 and the T-2 samples are amorphous without any visible lattice fringes, except an enhanced fluctuation in contrast in the image of T-2 (Fig. 1a and b). This means that T-2 is more heterogeneous in short-range arrangement of the atoms. Dissimilarly, clear lattice fringes can be seen in the HRTEM image of T-3 (Fig. 1c), suggesting the existence of nanocrystals. Evidently, decreasing the cooling rate enhances the short-range ordering in the microstructure.

DSC curves of the as-cast plates are shown in Fig. 2. Glass transition temperature T_g and onset temperature of crystallization T_x for three types of plates are essentially the same within the experimental error, indicating a comparable thermal stability among them. However, by carefully integrating the area covered by the crystallization peak in the DSC curve, different crystallization enthalpies were obtained. They are 53.2, 52.3, and 48.3 J/g for the T-1, T-2, and T-3 plates, respectively, also confirming an increasing ordering in microstructure with a decreasing cooling rate. The crystallization fraction of the sample, which reflects the degree of ordering, can be evaluated by calculating the ratio of the crystallization enthalpies from DSC curves [21]:

$$V_f = \frac{\Delta H_{max} - \Delta H}{\Delta H_{max}} \quad (1)$$

where ΔH_{max} is the total enthalpy change when the fully amorphous alloy transforms into a completely crystallized one, and ΔH is the crystallization enthalpy of the examining sample. Among the three thicknesses of plates, T-1 can be seen to be fully amorphous with zero crystallization fraction. The crystallization enthalpy of T-2 is slightly different from that of T-1, suggesting a negligible crystalline content in the T-2 sample. The small decrease in crystallization enthalpy results from the enhanced short-range ordering. However, the V_f of T-3 reaches 9.2%, indicating that it is a composite of glassy matrix embedded with nanocrystals. The inset of Fig. 2 is a local amplification of the DSC curves below the glass transition temperature, illustrating the heat release events due to structural relaxation. The relaxation enthalpy was calculated to be 4.4, 1.8, and 1.4 J/g for T-1, T-2, and T-3, respectively. A higher cooling rate has resulted in a larger relaxation enthalpy.

Fig. 3 displays the bending stress–displacement curve measured with the 1 mm × 3 mm × 40 mm bend specimen. The bend specimens produced from the different thicknesses of the as-cast plates exhibit a similar elastic displacement D_e (about 1.60 mm) but different average plastic displacement $\bar{D}_p$ prior to failure. The $\bar{D}_p$ of T-1, T-2, and T-3 is 2.11 ± 0.17, 1.11 ± 0.18 and 1.44 ± 0.16 mm, respectively. The corresponding average maximum bending stress

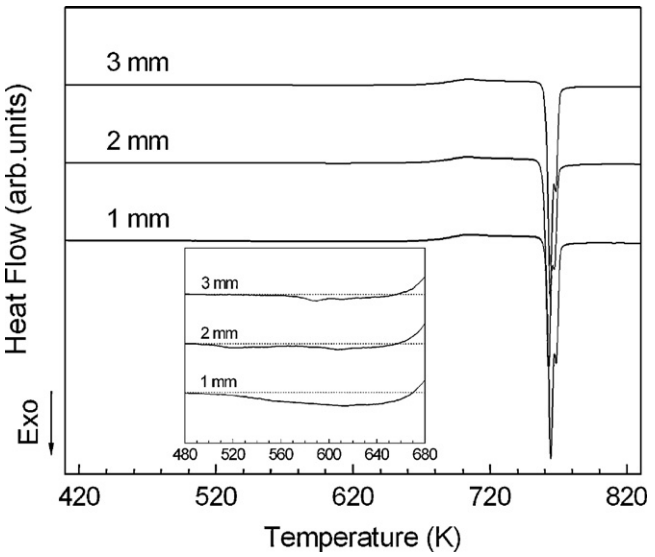

Fig. 2. DSC curves of the as-cast plates with different thicknesses at a heating rate of 20 K/min. The inset is an enlargement of the part below the glass transition temperature.

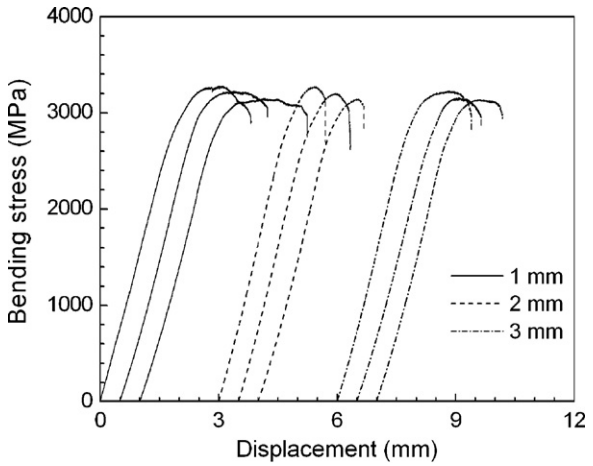

Fig. 3. Bending stress–displacement curves when the 1 mm × 3 mm × 40 mm bend specimens were machined from the as-cast plates of 1, 2 and 3 mm thicknesses.

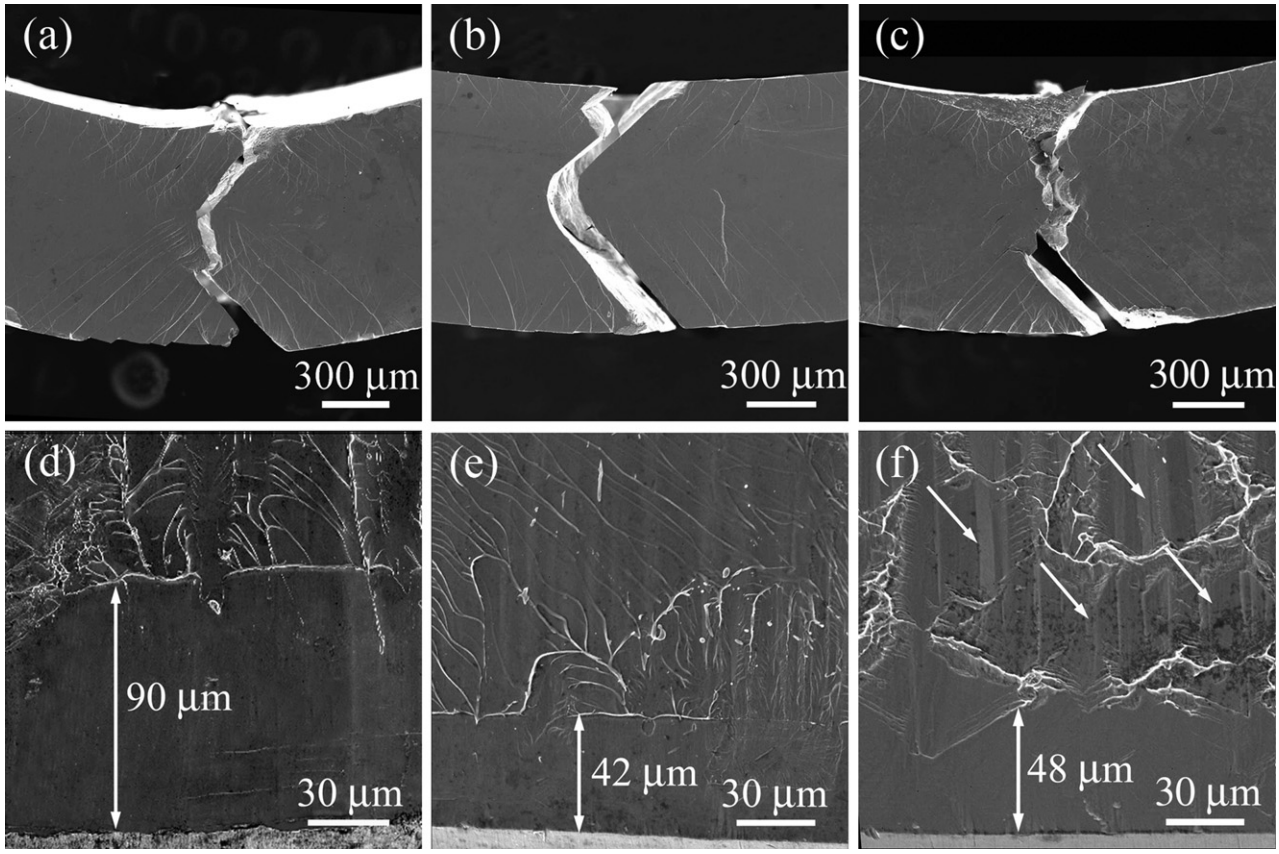

Fig. 4. SEM image of the side surface of the bend specimen and the initial shear region of the fracture surface on the tensile side after bend test. The corresponding original as-cast sample is 1 mm (a, d), 2 mm (b, e) and 3 mm (c, f) in thicknesses.

$\bar{\sigma}_m$ is 3206, 3195, and 3164 MPa, respectively. Considering that the bend specimens have the same geometry and the tests were performed under the same loading conditions, these results well reflect the mechanical property: a "large–small–large" transition in the bending plasticity of the as-cast $Zr_{55}Al_{10}Ni_5Cu_{30}$ BMGs with the decreasing cooling rate.

Shear band distributions on the side surface of the specimen subjected to bend test are shown in Fig. 4a–c. Besides secondary shear bands between the primary shear bands, several distinct shear offsets along the primary shear bands on the tensile side are observed. The density of shear bands is found to be the highest on the side surface of T-1 (Fig. 4a), the lowest on T-2 (Fig. 4b) and middle on T-3 (Fig. 4c). That is to say, a higher bending plasticity corresponds to a larger shear band density.

During bend test, the tensile side takes the main responsibility for the failure of the specimen. The initial shear region on the fracture surface was therefore examined, and the results are shown in Fig. 4d–f. A smooth region and a vein-like pattern region are found on all fracture surfaces. The former was caused by shear sliding [22] while the latter by the subsequent catastrophic failure [23]. The width of the smooth region is equal to the critical shear offset, which is a parameter directly reflecting the stable shear capability [22]. Among the specimens, T-1 has the largest shear offset of about 90 μm (Fig. 4d), while T-2 has the smallest one of about 42 μm (Fig. 4e). Interestingly, there are many slip traces (indicated by arrows) surrounded by vein-like pattern for T-3 (Fig. 4f).

4. Discussion

During the three point bending test, the first shear band, which coincides with the onset of plastic deformation, forms at the middle region of the tensile side (bottom surface), since yield is generally initiated at this region. As the strain increases, there are two main manners to sustain the plastic deformation: formation of new shear bands or sliding along the existing primary bands [24]. When the sliding displacement (shear offset) exceeds a critical value, the shear band is transformed into a crack, and then catastrophic fracture occurs [25]. Therefore, promoting the initiation of shear bands, enhancing the shear displacement and preventing shear bands from cracking are helpful to improve the plasticity of metallic glasses.

Generally, free volume is employed to explain the plasticity of metallic glasses on the basis of the following two points of view [17,26]. On one hand, sites with high free volume content favor nucleation and branching of shear bands. The concurrent nucleation of multiple shear bands and high branching of the shear bands are beneficial to sustain strain. On the other hand, a large amount of free volume helps to enhance the atomic mobility, which can alleviate the stress concentration and therefore prevent the metallic glass from cracking and/or breaking, i.e. promote to accommodate strain before failure.

Slipenyuk and Eckert [27] have demonstrated that the amount of free volume in metallic glasses is proportional to the enthalpy released during structural relaxation. As shown in the inset of Fig. 2, the enthalpy of structural relaxation follows a decreasing order of T-1, T-2 and T-3, i.e. the higher the cooling rate, the larger the relaxation enthalpy, and consequently the larger the free volume content in the metallic glass. Among the three types of specimens, T-1 contains the most free volume and has the highest shear band density as well as the largest shear offset, leading to the best bending plasticity. However, T-3 with the least free volume content exhibits a better plasticity than T-2, indicating that free volume

is not the only factor that affects the plasticity of metallic glasses. Other factors such as structural heterogeneity should also be considered.

The plasticity improvement of BMGs containing small nanocrystals can be ascribed to two factors [21]. Firstly, nanocrystals can act as obstacles hindering the propagation of shear bands and cracks. Secondly, the interface between the nanocrystal and the glassy matrix tends to create stress concentration, which is beneficial to the nucleation and multiplication of shear bands. One may argue that the nanocrystallization induced by isothermal annealing does not necessarily lead to improved plasticity [11]. In the present case, however, when nanocrystals precipitated during solidification, sufficient free volume was also kept in the amorphous matrix, therefore leading to an improved plasticity.

Based on the above discussion, two aspects should be taken into account in analyzing the correlation between the plasticity and the microstructure of BMGs. On one hand, for metallic glasses without nanocrystals, free volume will be the decisive factor, and reduction of free volume always leads to a degradation of plasticity [28]. On the other hand, for metallic glasses with finite volume fraction of nanocrystals, free volume still plays a role while nanocrystallization tends to enhance the plasticity. In our work, crystalline phase is hardly detected in T-1 and T-2, as evidenced by the large crystallization enthalpies as well as the HRTEM images. But the free volume content in T-2 decreases notably due to the lower cooling rate, determining that T-2 exhibits rather poor bending plasticity. Comparing to T-2, small nanocrystals form in T-3, evidenced by an obvious decrease in crystallization enthalpy and the lattice fringes in the HRTEM image (Fig. 1c). Considering that the free volume reduction from T-2 to T-3 is rather limited, the positive effect from nanocrystals overcomes the detrimental effect of the free volume reduction in T-3. In one word, as the cooling rate decreases, free volume content reduces while short-range ordering is enhanced in the as-cast metallic glasses. The competitive effect of these two factors leads to a transition of "large–small–large" in the bending plasticity of $Zr_{55}Al_{10}Ni_5Cu_{30}$ BMGs. Enhancing the short-range order in microstructure while not resulting in nanocrystallizing in the amorphous matrix will significantly deteriorate the plasticity of a metallic glass.

Recently, Kumar et al. [29] compared the bending plasticity of Pd-based and Pt-based bulk metallic glasses. They found that low cooling rates during casting render Pd-BMG ($Pd_{43}Cu_{27}Ni_{10}P_{20}$) brittle, whereas Pt-BMG ($Pt_{57.5}Cu_{14.7}Ni_{5.3}P_{22.5}$) retains high plasticity at all cooling rates. This also indicates that both free volume and topological arrangement of atoms in metallic glasses should be taken into account in studying the plasticity of BMGs.

5. Conclusions

The effect of cooling rate on the plasticity of $Zr_{55}Al_{10}Ni_5Cu_{30}$ BMG was investigated in terms of the correlation between bending plasticity and the microstructure of the as-cast samples with different thicknesses. It is found that as the cooling rate decreases, the short-range ordering in the microstructure is enhanced, leading to nanocrystallization in the glassy matrix at the expense of reduced free volume. The comprehensive effect of free volume and short-range ordering results in a "large–small–large" transition in the bending plasticity of the $Zr_{55}Al_{10}Ni_5Cu_{30}$ BMGs.

Acknowledgments

The authors would like to acknowledge the National Natural Science Foundation of China (Grant No. 50771064 and 50831003) and the National Basic Research Program of China (Grant No. 2011CB610405) for financial supports.

References

[1] W.H. Wang, C. Dong, C.H. Shek, Mater. Sci. Eng. R 44 (2004) 45.
[2] C.A. Schuh, T.C. Hufnagel, U. Ramamurty, Acta Mater. 55 (2007) 4067.
[3] A.R. Yavari, J.J. Lewandowski, J. Eckert, MRS Bull. 32 (2007) 635.
[4] J. Eckert, J. Das, S. Pauly, C. Duhamel, J. Mater. Res. 22 (2007) 285.
[5] J. Schroers, Adv. Mater. 22 (2010) 1566.
[6] K.F. Yao, F. Ruan, Y.Q. Yang, N. Chen, Appl. Phys. Lett. 88 (2006) 122106.
[7] J.C. Oh, T. Ohkubo, Y.C. Kim, E. Fleury, K. Hono, Scripta Mater. 53 (2005) 165.
[8] E.S. Park, D.H. Kim, Acta Mater. 54 (2006) 2597.
[9] H. Kato, K. Yubuta, D.V. Louzguine, A. Inoue, H.S. Kim, Scripta Mater. 51 (2004) 577.
[10] A. Inoue, W. Zhang, T. Tsurui, A.R. Yavari, A.L. Greer, Philos. Mag. Lett. 85 (2005) 221.
[11] T. Ohkubo, D. Nagahama, T. Mukai, K. Hono, J. Mater. Res. 22 (2007) 1406.
[12] K. Mondal, T. Ohkubo, T. Toyama, Y. Nagai, M. Hasegawa, K. Hono, Acta Mater. 56 (2008) 5329.
[13] Z.W. Zhu, S.J. Zheng, H.F. Zhang, B.Z. Ding, Z.Q. Hu, P.K. Liaw, Y.D. Wang, Y. Ren, J. Mater. Res. 23 (2008) 941.
[14] F.O. Méar, T. Wada, D.V. Louzguine-Luzgin, A. Inoue, Philos. Mag. Lett. 89 (2009) 276.
[15] Y.J. Huang, J. Shen, J.F. Sun, Appl. Phys. Lett. 90 (2007) 081919.
[16] J. Shen, Y.J. Huang, J.F. Sun, J. Mater. Res. 22 (2007) 3067.
[17] L.Y. Chen, A.D. Setyawan, H. Kato, A. Inoue, G.Q. Zhang, J. Saida, X.D. Wang, Q.P. Cao, J.Z. Jiang, Scripta Mater. 59 (2008) 75.
[18] Y. Hu, J.F. Li, T. Lin, Y.H. Zhou, J. Mater. Res. 24 (2009) 3590.
[19] G. Kumar, T. Ohkubo, K. Hono, J. Mater. Res. 24 (2009) 2353.
[20] N. Chen, D. Pan, D.V. Louzguine-Luzgin, G.Q. Xie, M.W. Chen, A. Inoue, Scripta Mater. 62 (2010) 17.
[21] L.C. Zhang, F. Jiang, D.H. Zhang, L. He, J. Sun, J.T. Fan, Z.F. Zhang, Adv. Eng. Mater. 10 (2008) 943.
[22] F.F. Wu, Z.F. Zhang, S.X. Mao, Acta Mater. 57 (2009) 257.
[23] Z.F. Zhang, J. Eckert, L. Schultz, Acta Mater. 51 (2003) 1167.
[24] T.C. Hufnagel, P. El-Deiry, R.P. Vinci, Scripta Mater. 43 (2000) 1071.
[25] R.D. Conner, W.L. Johnson, N.E. Paton, W.D. Nix, J. Appl. Phys. 94 (2003) 904.
[26] F. Jiang, Y.L. Zhao, L.C. Zhang, S.B. Pan, Y.G. Zhou, L. He, J. Sun, Adv. Eng. Mater. 11 (2009) 374.
[27] A. Slipenyuk, J. Eckert, Scripta Mater. 50 (2004) 39.
[28] M. Wakeda, Y. Shibutani, S. Ogata, J. Park, Intermetallics 15 (2007) 139.
[29] G. Kumar, S. Prades-Rodel, A. Blatter, J. Schroers, Scripta Mater. 65 (2011) 585.